



Improved height correction model for hydrostatic mapping functions in GNSS data processing

Xiaochuan Qu^{1,2} · Wenwu Ding³ · Felix Norman Teferle⁴ · Yunbin Yuan³ · Tingye Tao^{1,2} · Yongchao Zhu^{1,2} · Shuiping Li^{1,2}

Accepted: 11 October 2022 / Published online: 10 December 2022
© Springer-Verlag GmbH Germany, part of Springer Nature 2022

Abstract

In precise global navigation satellite system (GNSS) data processing, the mapping function is a key factor in troposphere delay modelling. Currently, site-dependent troposphere mapping functions are only provided for specific sites, while for other sites, other mapping functions, such as the gridded Vienna Mapping Function (VMF1/VMF3), are recommended, in which a height correction is always required to convert the hydrostatic mapping function from model height to site height. In this analysis, an improved height correction model is proposed based on the fifth-generation European Centre for Medium-Range Weather Forecasts reanalysis (ERA5). Compared to the commonly used Niell model, the coefficients in the improved model are no longer constants but are provided in a global $5^\circ \times 5^\circ$ grid on a monthly basis, with the significant difference that the coefficient a of the Niell model is modelled as quadratically varying with height. To evaluate its performance, we applied the improved model to VMF1 ($2^\circ \times 2.5^\circ$) and VMF3 ($5^\circ \times 5^\circ$ and $1^\circ \times 1^\circ$) gridded data for all of 2015 and then compared them with site-dependent data at 402 VMF1 sites and 505 VMF3 sites, respectively. It was shown that the improved model outperformed the Niell model at most stations, and the improvement of the slant path delay (SPD) became better with increasing height difference. The maximum improvement of the SPD at a 3° elevation angle is 29.5 mm at SANT for the VMF1 $2^\circ \times 2.5^\circ$ grid and 18.7 mm and 16.4 mm for the VMF3 $5^\circ \times 5^\circ$ and $1^\circ \times 1^\circ$ grids, respectively, both achieved at NAMA. For all height difference intervals, the average and maximum improvements of the SPD can reach approximately 30% and 50% for both the VMF1 $2^\circ \times 2.5^\circ$ and VMF3 $1^\circ \times 1^\circ$ grids, respectively, while only approximately 14% and 30% improvements for the VMF3 $5^\circ \times 5^\circ$ grid, respectively, due to the coarse resolution of the mapping function. Therefore, we can benefit significantly from the improved model, which becomes even more important when stations with large height differences, i.e. in mountainous areas or on mid-ocean islands, are included in precise GNSS data processing.

Keywords Height correction · VMF1/VMF3 · Hydrostatic mapping function · Troposphere delay · GNSS

1 Introduction

For space geodetic measurements, when a radio signal travels through the troposphere, it slows down and the propagation path bends, thus causing tropospheric delay. As a major error source, this delay is usually separated into hydrostatic and nonhydrostatic (wet) parts (Davis et al. 1985; Boehm et al. 2006b):

$$\Delta L = \Delta L_h^z \Delta m_{f_h} + \Delta L_w^z \Delta m_{f_w} \quad (1)$$

where ΔL_h^z and ΔL_w^z represent the zenith hydrostatic delay (ZHD) and zenith wet delay (ZWD), respectively, and m_{f_h} and m_{f_w} are the hydrostatic and wet mapping functions.

✉ Wenwu Ding
bindingboy@gmail.com

¹ School of Civil Engineering, Hefei University of Technology, Hefei 230009, People's Republic of China

² Anhui Key Laboratory of Civil Engineering Structures and Materials, Hefei University of Technology, Hefei 230009, People's Republic of China

³ State Key Laboratory of Geodesy and Earth's Dynamics, Innovation Academy for Precision Measurement Science and Technology, Chinese Academy of Sciences (CAS), Wuhan 430077, People's Republic of China

⁴ Geophysics Laboratory, University of Luxembourg, Luxembourg City, Luxembourg

In precise data processing, ZHD can be calculated accurately from empirical models or numerical weather models (NWMs) (Zhang et al. 2021), while ZWD is usually estimated as an unknown. Since errors in the mapping functions directly influence the modelling accuracies of the tropospheric delay (Boehm et al. 2006a; Ning et al. 2016), they have been an important topic and have attracted much attention. To date, researchers have built several mapping functions, such as the Niell Mapping Function (NMF) (Niell 1996), Isobaric Mapping Function (IMF) (Niell 2000), Global Mapping Function (GMF) (Boehm et al. 2006a) and Vienna Mapping Functions (VMF1/VMF3) (Boehm and Schuh 2004; Boehm et al. 2006b; Landskron and Boehm 2018; Urquhart et al. 2014), among which VMF1/VMF3, calculated by the ray-tracing technique through NWMs provided by the European Centre for Medium-Range Weather Forecasts (ECMWF), is assumed to be the most accurate (Boehm et al. 2009; Landskron and Boehm 2018). In VMF1/VMF3, the following third term fraction form is adopted (Boehm et al. 2006b):

$$mf(e) = \frac{1 + \frac{a}{1 + \frac{b}{1+c}}}{\sin e + \frac{a}{\sin e + \frac{b}{\sin e + c}}} \quad (2)$$

where e is the elevation angle, and coefficients a , b and c are different for the hydrostatic and wet mapping functions. In VMF1, the coefficients b and c are both constants, while the hydrostatic coefficient c depends on the station latitude and day of year (Boehm et al. 2006b). By comparison, annual and semiannual variations in coefficients b and c are modelled in VMF3 to improve the accuracies in mountainous areas (Landskron and Boehm 2018).

At present, site-dependent and gridded VMF1/VMF3 data are provided and available at <https://vmf.geo.tuwien.ac.at/> (Landskron and Boehm 2018). The site-dependent mapping functions are calculated directly at specific stations and are only provided for International GNSS Service (IGS), Very Long Baseline Interferometry (VLBI), Satellite Laser Ranging (SLR) and Doppler Orbitography and Radio-positioning Integrated by Satellite (DORIS) stations. For other stations not included in these networks, researchers are recommended to use the gridded VMF1/VMF3 data. Currently, gridded data are provided at three resolutions for user applications: $2.0^\circ \times 2.5^\circ$ for VMF1 and both $5^\circ \times 5^\circ$ and $1^\circ \times 1^\circ$ for VMF3 (Landskron and Boehm 2018). The mapping functions for any sites globally can then be calculated horizontally through bilinear interpolation with four surrounding points of the gridded data.

Due to the strong dependences of ZHD/ZWD and the mapping functions on heights, height corrections in tropospheric models are always required to convert them from model height to site height, as done in VMF1/VMF3 (Kouba 2008),

GMF and GPT2 (Boehm et al. 2006a; Lagler et al. 2013). Researchers have built accurate models for ZHD/ZWD height corrections; for example, Kouba (2008) proposed the ZHD height correction model adopted in VMF1/VMF3 by considering the height dependence of atmospheric pressure. A new ZWD vertical approach proposed by Dousa and Elias (2014) takes an exponential decay parameter γ as input, rather than a water vapour pressure decreasing factor as adopted in the UNB3 model (Collins and Langley 1997), and outperforms the existing ZWD methods by a factor of 2 to 3. Modelling the annual and semiannual variations in inverse scale height, Lou et al. (2018) built a zenith total delay (ZTD) exponential model in China. Compared with ZHD/ZWD, very little research has been done on the height correction of mapping functions, and until now, there has been no height correction model for the wet mapping function due to an assumption of its independence from station height, while the empirical height correction model proposed by Niell (1996) (hereafter called the Niell model) is usually applied to the hydrostatic mapping function and can be expressed as follows:

$$\Delta mf_h = H \cdot \left(\frac{1}{\sin e} - \frac{1 + \frac{a_{ht}}{1 + \frac{b_{ht}}{1+c_{ht}}}}{\sin e + \frac{a_{ht}}{\sin e + \frac{b_{ht}}{\sin e + c_{ht}}}} \right) \quad (3)$$

where H is the station height in kilometres and a_{ht} , b_{ht} and c_{ht} are the coefficients calculated based on the climatology by Niell (1996). The Niell model is widely adopted in gridded VMF1/VMF3, GMF and GPT2. However, the constant values of these coefficients, calculated by the least squares method using values at nine elevation angles and then averaged spatially over five latitudes and temporally over nine standard profiles, are not accurate enough to account for variations in mapping functions with heights, especially considering that the accuracies of NWMs and mapping functions have been greatly improved. Zus et al. (2015) indicated that when utilizing the Niell model, the residual errors of slant hydrostatic delay at a 3° elevation angle can reach up to 50 mm for users located 2 km above the orography. Landskron and Boehm (2018) also noted the importance of a new height correction model to enhance tropospheric modelling accuracies in precise GNSS data processing.

In this analysis, we establish an improved height correction model for the hydrostatic mapping function. The paper is organized as follows: Sect. 2 introduces the methods and data adopted in the manuscript. Section 3 evaluates the internal modelling accuracies and external accuracies of the correction model applied to gridded VMF1/VMF3. Section 4 discusses the performance of our proposed improved model, and conclusions are provided in Sect. 5.

2 Data and method

In this section, the NWM data and method used to calculate the tropospheric mapping functions, together with the form and generation method of the improved correction model, are introduced.

2.1 NWM and calculation of tropospheric mapping functions

The fifth-generation ECMWF reanalysis (ERA5) data (<https://cds.climate.copernicus.eu/>) (Hersbach et al. 2019), the latest reanalysis product, were adopted to calculate mapping functions in this analysis. ERA5 monthly averaged parameters of relative humidity, temperature and geopotential on 37 pressure levels were used to calculate the neutral atmospheric refractivity. Before calculation, several transformations should be applied to the ERA5 parameters, including converting geopotentials to geodetic heights using the Somigliana equation (Mahoney 2005) and Earth Gravitational Model 1996 (EGM96), and converting relative humidity values to water vapour pressures according to saturation vapour pressures (World Meteorological Organization 2012). Then, the refractivity can be obtained using a radio refractive index formula with the ‘best average’ coefficients (Rüeger 2002). Under the assumption of a local spherical symmetric atmosphere, tropospheric delay at any elevation angle can be calculated by in-house ray-tracing software developed based on the 4th-order Runge–Kutta method (Qu et al. 2015). For consistency, the same strategies for calculating coefficients b and c for VMF1/VMF3 were adopted when generating the improved height correction model for VMF1/VMF3. However, coefficient a was estimated from a single averaged delay over several azimuths at an outgoing elevation of 3° , adopted in the gridded and site-dependent VMF3 (Landskron and Boehm 2018), rather than at the initial elevation of 3.3° as done in VMF1.

2.2 Establishment of the improved height correction model

According to the empirical equation of the Niell model (Eq. 3), it is assumed that mf_h varies linearly with height, and such variations are temporally constant. However, actual variations in mf_h are more complex and time dependent. To be more accurate, in this analysis, a refined model denoted as HCHMF-2 (Height Correction of Hydrostatic Mapping Function: the number ‘2’ means quadratic form of coefficient a) is established, assuming that the coefficient a_{ht} in Eq. (3) varies quadratically with height (Eq. 4).

$$\Delta mf_h = H \cdot \left(\frac{1}{\sin e} - \frac{1 + \frac{a_1 H^2 + a_2 H + a_3}{1 + \frac{b_{ht}}{1 + c_{ht}}}}{\sin e + \frac{a_1 H^2 + a_2 H + a_3}{\sin e + \frac{b_{ht}}{\sin e + c_{ht}}}} \right) \quad (4)$$

where a_1, a_2, a_3, b_{ht} and c_{ht} are the height correction model coefficients.

Coefficients of the proposed height correction model are provided in a gridded type. The fitting height interval (from mean sea level (MSL) to 5 km above MSL applied in this analysis), an important factor in establishing the model, should be selected to guarantee that nearly all possible users are located within this interval, so the extrapolation errors when using the model can be avoided. Using the monthly averaged ERA5 data in 2015, we calculated four groups of HCHMF-2 coefficients fitted within different height intervals (from MSL to 2 km, 3 km, 4 km and 5 km above MSL). Taking the mapping functions calculated directly at different heights as reference, the maximum and average root mean square (RMS) of the slant path delay (SPD), equal to mf_h multiplied by ZHD, errors for the 3° elevation angle at different heights using different groups of coefficients are shown in Figure S1 in the supplementary material. We find that the extrapolation errors can reach up to tens of millimetres, which cannot be ignored. Additionally, due to the different orography files adopted in VMF1/VMF3, different height correction models must be provided separately if we adjust the fitting interval based on the orography height. The refractive index from the orography of ERA5 downwards to MSL is calculated by exponential extrapolation, which will result in some errors in the modelling coefficients. To evaluate its impact, two HCHMF-2 models, fitted using the mapping functions from orography and from MSL to 5 km above MSL, denoted as HCHMF-2 (Orography) and HCHMF-2 (MSL), respectively, are calculated. Taking the site-dependent VMF3 as reference, the performances of these two models when applied to the VMF3 $5^\circ \times 5^\circ$ grid are compared, and the differences in the RMS of the SPD errors at the 3° elevation angle in 2015 are shown in Figure S2 in the supplementary material. The RMS increases are not larger than 1.4 mm for all those IGS stations when using the HCHMF-2 (MSL) model. However, for those stations below the orography of ERA5, the RMS can increase up to 58.2 mm when using the HCHMF-2 (Orography) model. Considering these factors, at each grid point, we calculated the tropospheric mapping functions every 100 m from MSL to 5 km above MSL, and the differences in mf_h at each height grid relative to that at MSL were obtained to calculate the coefficients in a least squares method with starting values of $a_1 = 0, a_2 = 0, a_3 = 0, b_{ht} = 0$ and $c_{ht} = 0$. The height correction model was calculated from monthly averaged ERA5 data every month, and provided on a global $5^\circ \times 5^\circ$ grid. The accuracies are slightly improved by providing the height correction model every day based on daily ERA5 data, but for

Table 1 Details of the three models for comparison in this analysis

Model	Expression	Spatial resolution	Temporal resolution
Niell model	Equation (3)	Single	Single
HCHMF-2 model	Equation (4)	$5^\circ \times 5^\circ$	Monthly
HCHMF-0 model	Equation (3)	$5^\circ \times 5^\circ$	Monthly

most stations, the improvements in the SPD are not larger than 4.0 mm at the 3° elevation angle (detailed results are provided in Figure S3 in the supplementary material). Thus, to balance the modelling accuracies and computational load, we elected to provide a monthly height correction model in this analysis. Height correction at any station can be obtained by bilinear interpolation in the horizontal plane with the four surrounding grid points, while the same set of monthly coefficients are used for any date within one month, which means that no temporal interpolation is needed.

To clearly show the effects of the proposed quadratic model (denoted as HCHMF-2), another model (denoted as HCHMF-0), expressed as Eq. (3) with coefficients recalculated using monthly ERA5 data, was also evaluated. Details of these three models are listed in Table 1 for comparison.

3 Results

In this section, we evaluate the internal accuracies of the quadratic model when calculating the coefficients, as well

as the external modelling accuracies when applied to the VMF1/VMF3 grids.

3.1 Internal modelling accuracies

We first calculated the internal modelling accuracies to evaluate their capabilities in modelling variations of the mapping function with height. Taking the mapping functions calculated from the monthly averaged ERA5 data every 100 m on a global $5^\circ \times 5^\circ$ grid as reference, we applied the height corrections using the Niell, HCHMF-0 and HCHMF-2 models to the mapping function calculated at the MSL of each grid and then compared them with the reference values. Thus, the monthly mf_h errors in 2015 are obtained for each height correction model at each height and grid. Figure 1 shows the RMS of the monthly SPD errors at the 3° elevation angle for different heights at two grid points: $(-27.5^\circ\text{S}, 20^\circ\text{E})$ and $(-77.5^\circ\text{S}, 130^\circ\text{E})$. It is clear that the RMS using the Niell model, with a maximum of approximately 50 mm at 5 km, increases gradually with height. The RMS using the HCHMF-0 model is smaller than 2 mm at the first grid point but can reach up to 21 mm for approximately 1.5 km above MSL at the second grid point. By comparison, the best performance is achieved using the HCHMF-2 model, of which the RMS is always smaller than 3 mm for all heights at these two grid points.

Figure 2 shows the RMS of the monthly SPD errors at a 3° elevation angle every 500 m above MSL on a global $5^\circ \times 5^\circ$ grid, as well as the maximum and average values. Note that different colour bar labels are used for the three models. Clearly, the global RMS using the Niell model

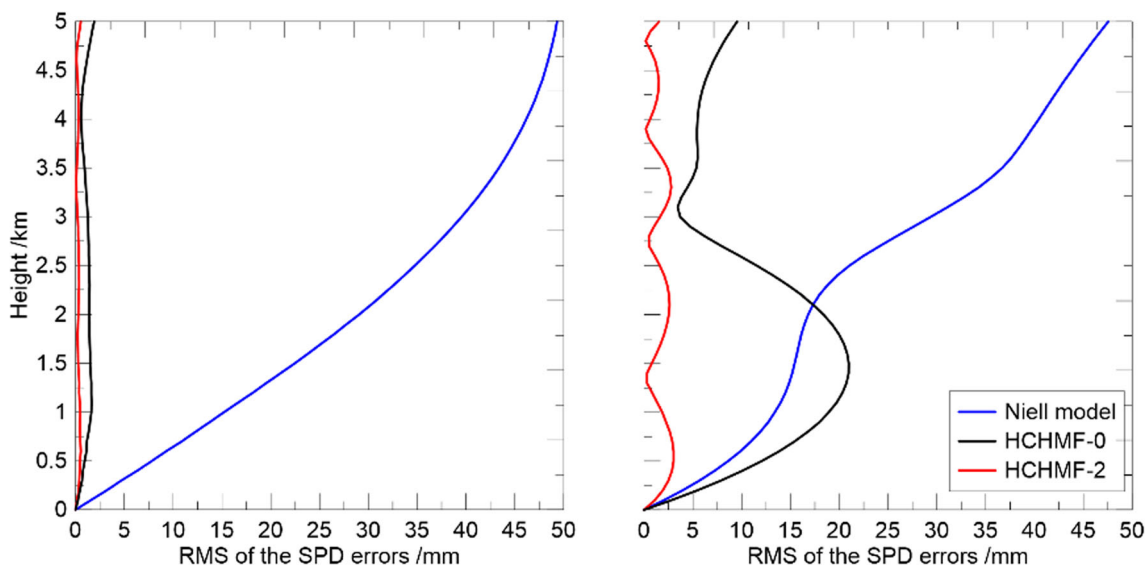


Fig. 1 RMS of the monthly SPD errors at the 3° elevation angle in 2015 using three models for different heights at $(-27.5^\circ\text{S}, 20^\circ\text{E})$ (left) and $(-77.5^\circ\text{S}, 130^\circ\text{E})$ (right). The blue curve represents the Niell model,

the black curve denotes the constant model (HCHMF-0), and the red curve shows the quadratic model (HCHMF-2)

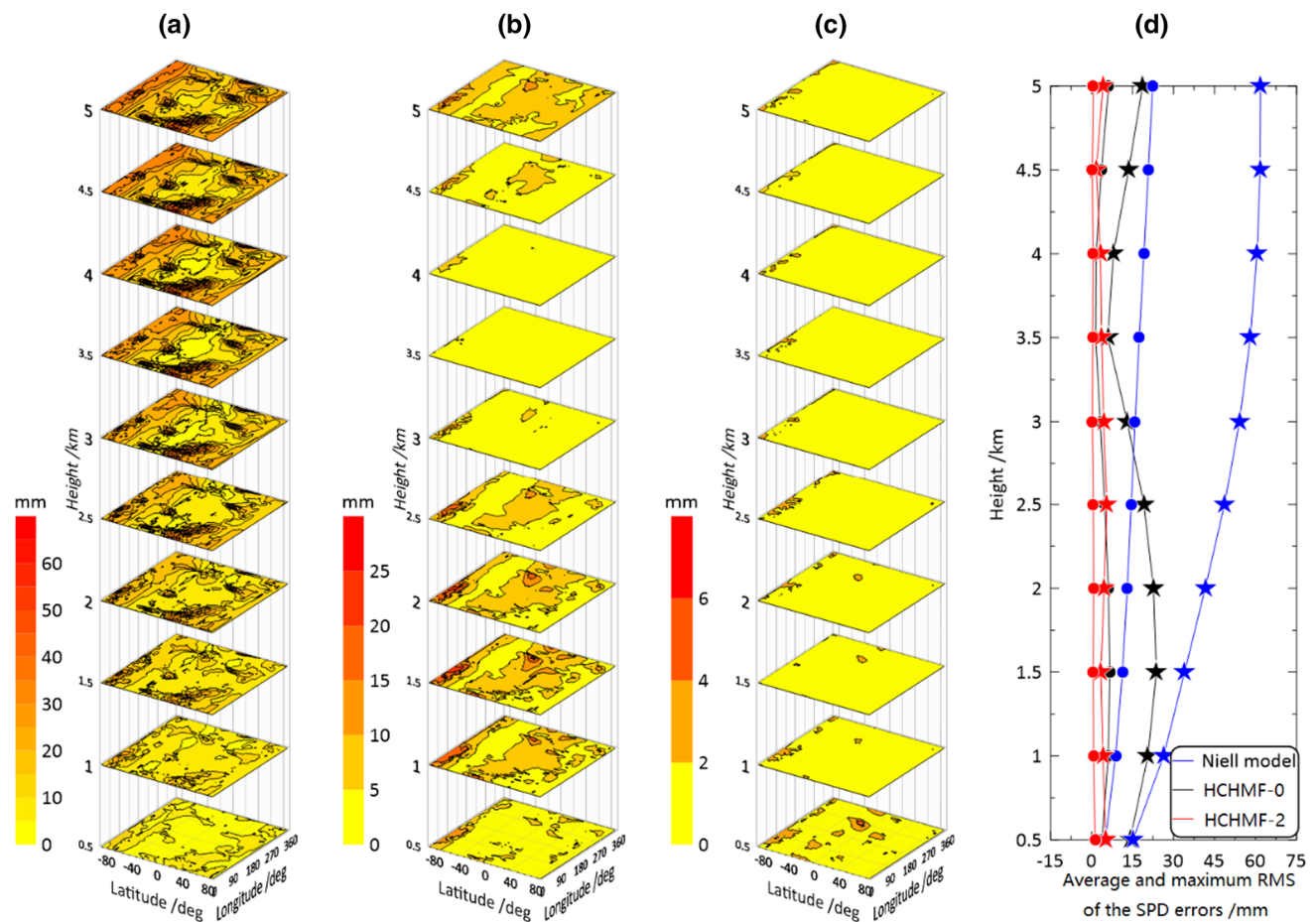


Fig. 2 RMS of the monthly SPD errors at the 3° elevation angle in 2015 every 500 m above MSL on a global 5° × 5° grid using the Niell model (a), HCHMF-0 model (b) and HCHMF-2 model (c), together with the maximum (indicated by pentagram) and average (indicated by circle) RMS at each height (d). For a–c, the colour bar represents

the global RMS value, yellow means smaller RMS and reddish means larger values. For the right panel (d), the different colours denote different models, among which the blue, black and red curves represent the Niell, HCHMF-0 and HCHMF-2 models, respectively

always increases with height, with the average RMS gradually increasing from 5.0 mm at 0.5 km to 22.3 mm at 5.0 km. Even at lower heights there are still large errors, especially for those points at mid and high latitudes. The maximum RMS can reach up to 34.0 mm at 1.5 km above MSL. When using the HCHMF-0 model, the accuracy is greatly improved, and the average RMS is smaller than 6.7 mm, confirming the importance of considering spatial and temporal differences in the mapping function variations with height. Nevertheless, we notice that the errors are still larger in some areas. For those stations approximately 1.5 km above MSL, the maximum and average RMS can reach 23.7 mm and 6.7 mm, respectively, indicating that the HCHMF-0 model cannot interpret well the variation in mapping functions with station height in some areas. By comparison, the HCHMF-2 model performs the best, with a maximum RMS of only 5.6 mm. In addition, the accuracies using the HCHMF-2 model are

comparable at different heights, and the average RMS is always approximately 1.0 mm.

3.2 External modelling accuracies

To evaluate the applicability of the quadratic height correction model to the popularly used VMF1 and VMF3 grids, we applied the improved model to gridded models and then compared them with site-dependent VMF1 and VMF3 data. A total of three gridded models, VMF1 (2.0° × 2.5°) and VMF3 (1° × 1° and 5° × 5°), were evaluated in this analysis. We downloaded the 6-hourly VMF1 and VMF3 data (UTC 00, 06, 12 and 18 h) for all of 2015 and ignored those stations with data fewer than 30 days. Thus, as shown in Fig. 3, the comparisons were actually conducted for 402 stations for VMF1 and 505 stations for VMF3. Using the VMF1/VMF3 orography files, we calculated the orography heights of stations by bilinear interpolation and then compared them with

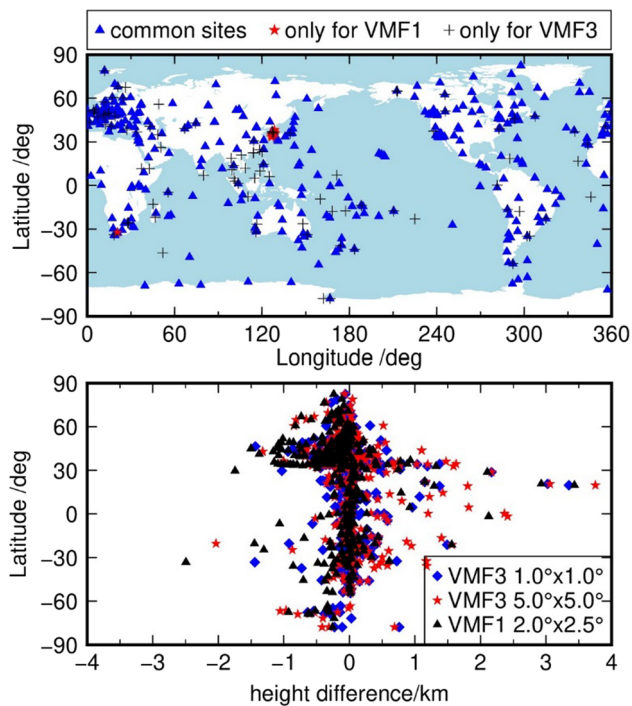


Fig. 3 Distribution of VMF1/VMF3 stations adopted in evaluating the external modelling accuracies (top) and height differences (negative value means station is below the model orography) between station and VMF1/VMF3 model orography (bottom)

station heights. Figure 3 plots the height differences between the station and its orography height. We observe that the height differences for the three gridded models are mostly in the range of ± 2.0 km, while reaching up to 3.5 km at MKEA (19.8°N , 204.5°E).

Since the gridded coefficient a_h is obtained by converting the hydrostatic mapping function mf_h from model orography to MSL using the Niell model (Landskron and Boehm 2018), the impact of the Niell model on the gridded VMF1 and VMF3 mf_h should be computed before evaluating the performance of the improved models. This is done as follows: mf_h is converted from MSL to orography using the Niell model and then converted to station height using the improved height correction model. After these transformations, mf_h , unaffected by the Niell model, can be compared with site-dependent VMF1 and VMF3 mapping functions.

Figure 4 shows the 6-hourly VMF1 SPD errors at the 3° elevation angle in 2015 for NAMA and AREQ, of which the height differences are approximately 1.3 km and -0.7 km, respectively. It is clear that when using the Niell model, there are still large systematic residual errors at both sites. The RMS of the SPD errors at the 3° elevation angle reaches 20 mm. Applying the HCHMF-0 model, the RMS can be reduced by approximately 72% at NAMA. However, the improvement is not obvious at AREQ, for which the RMS is

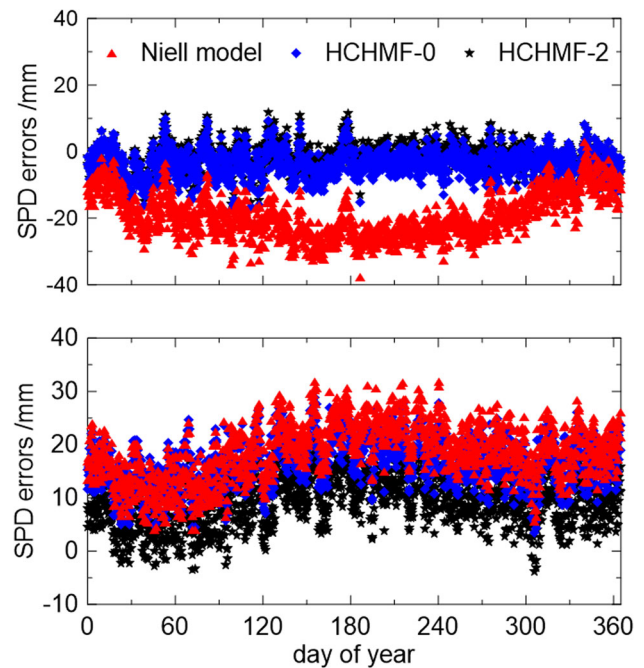


Fig. 4 6-hourly VMF1 SPD errors at the 3° elevation angle for NAMA (19.2°N , 42.0°E) (top) and AREQ (-16.5°S , 288.5°E) (bottom) in 2015. The different symbols represent different models (red triangle: Niell model, blue square: HCHMF-0, black star: HCHMF-2)

still 17.0 mm. The different performances using the HCHMF-0 model for AREQ and NAMA suggest that the correction model based on Eq. (3) may not exactly represent the variation in mf_h with height globally. Comparatively, the best results are achieved using the HCHMF-2 model, of which the RMS is 4.8 mm and 10 mm for NAMA and AREQ, respectively.

Figure 5 depicts the RMS of the 6-hourly SPD errors at the 3° elevation angle in 2015 for 402 VMF1 sites and 505 VMF3 sites. When the height differences are small, especially within ± 0.5 km, comparable performances can be achieved using all three height correction models except that the RMS at the VMF1 site AIRA (31.8°N , 130.6°E) reaches 56 mm, which requires further investigation. The average RMS for the VMF1 $2^\circ \times 2.5^\circ$ and VMF3 $1^\circ \times 1^\circ$ grids is 6.6 mm and 2.5 mm, respectively, and becomes slightly worse for the VMF3 $5^\circ \times 5^\circ$ grid due to the coarse resolution. When the height difference becomes larger, the accuracy using the Niell model decreases rapidly. The maximum RMS for the VMF1 $2^\circ \times 2.5^\circ$ and VMF3 $1^\circ \times 1^\circ$ grids reaches 48 mm and 26 mm, respectively, both arising at SANT (-33.1°S , 289.3°E), while it is 35 mm at IQQE (-20.3°S , 289.9°E) for the VMF3 $5^\circ \times 5^\circ$ grid. The height differences at these sites are all larger than 1.4 km. The performances can be improved with the refined models. Comparing the RMS using the Niell and HCHMF-2 models, maximum improvements of 18 mm,

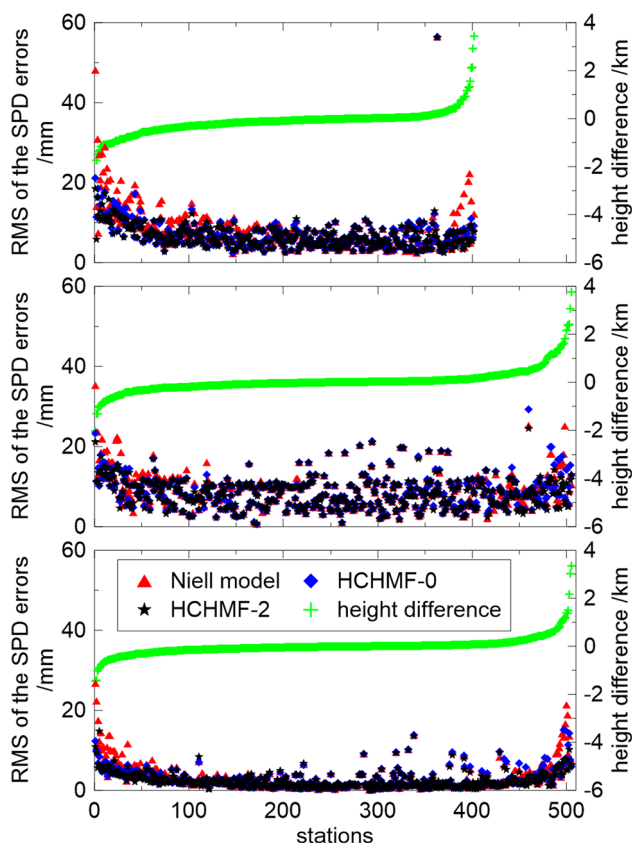


Fig. 5 RMS of the 6-hourly SPD errors at the 3° elevation angle for 402 VMF1 sites (top) and 505 VMF3 sites (middle: 5° × 5° grid, bottom: 1° × 1° grid) in 2015. Units of RMS and height differences are mm and km, respectively. The red triangles, blue squares and black stars represent the Niell, HCHMF-0 and HCHMF-2 models, respectively, while the green pluses denote the height difference between station height and corresponding orography height

24 mm and 14 mm can be achieved when applied to the VMF1 and VMF3 5° × 5°/1° × 1° grids, respectively.

Figure 6 plots the average RMS of the 6-hourly SPD errors for the 3° elevation angle at five intervals according to distinct height differences. The improvement using the HCHMF-0 and HCHMF-2 models becomes obvious with increase in height differences. When applying the HCHMF-2 model to the VMF1 2° × 2.5° and VMF3 1° × 1° grids, the average improvements reach approximately 30% at all intervals, and the largest improvement achieves approximately 50% within intervals of 2–3 km and 1–2 km, respectively. However, the average and largest improvements for the VMF3 5° × 5° grid are only approximately 14% and 30%, respectively, due to a coarser resolution. Compared with the HCHMF-2 model, the HCHMF-0 model exhibits a slightly smaller improvement, especially within the interval of 1–3 km for the VMF3 grids. The average improvements for these three grids based on the HCHMF-0 model are approximately 26%, 5% and 18%, respectively.

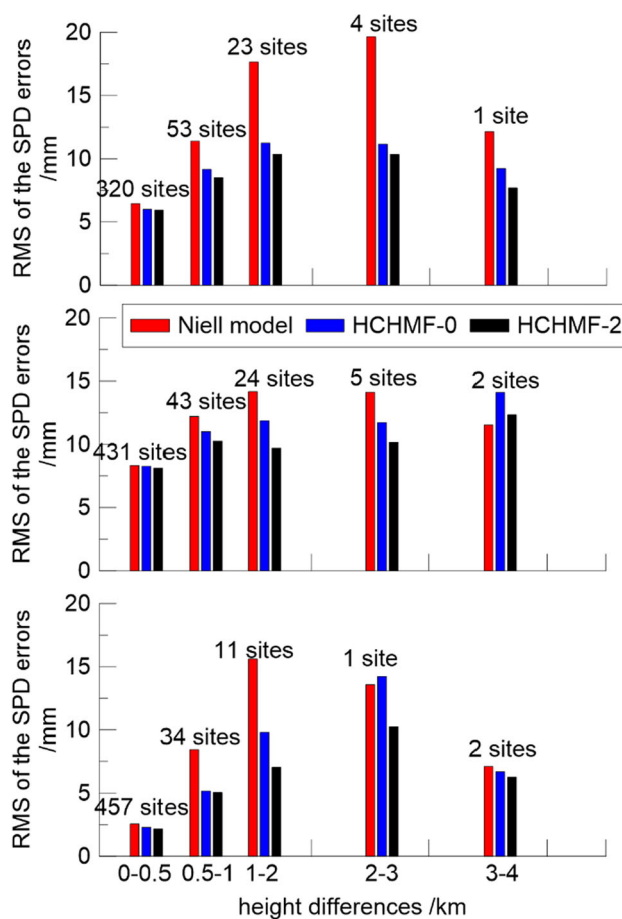


Fig. 6 Average RMS of the 6-hourly SPD errors in 2015 for stations within distinct height differences at the 3° elevation angle for the VMF1 2° × 2.5° (top) and VMF3 5° × 5° (middle)/1° × 1° (bottom) grids. The different colours represent different models (red: Niell, blue: HCHMF-0, black: HCHMF-2). The number of sites represents the number of stations within each interval according to height differences

To clearly investigate the reliability of the improved models, histograms for the differences in the RMS of the SPD errors at the 3° elevation angle using two models with respect to the Niell model are shown in Fig. 7. Improvements can be achieved at most stations, especially when employing the VMF3 1° × 1° grid. Additionally, for those stations whose performance worsens, the magnitudes are all within 5 mm. We also plot the actual values in Fig. 7 of those stations at which the RMS differences are larger than 5 mm. There are 38, 18 and 19 stations for the VMF1 2° × 2.5° and VMF3 5° × 5°/1° × 1° grids, respectively, with height differences varying from approximately 0.4 to 2.5 km. The improvements using the HCHMF-2 model can reach up to approximately 8 mm at several stations where the height differences are approximately 0.5 km, indicating that the improved models are also necessary for those stations with small height differences. Compared with the HCHMF-2 model, the performances using the HCHMF-0 model are mostly the same

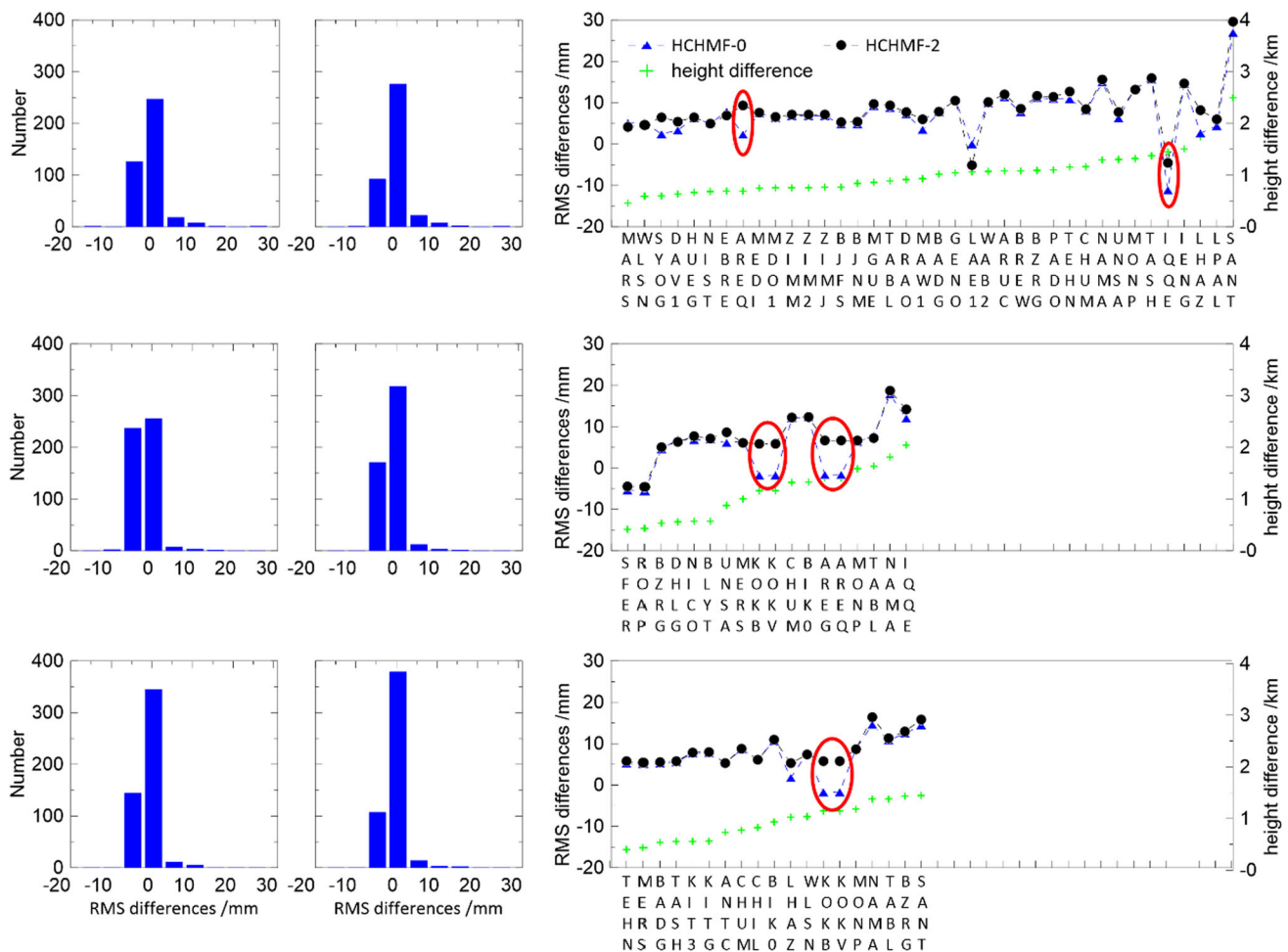


Fig. 7 Histograms of the differences in the RMS of the 6-hourly SPD errors at the 3° elevation angle in 2015 between the HCHMF-0 (left panels)/HCHMF-2 (middle panels) models and the Niell model, together with the absolute RMS differences larger than 5 mm (right panels) for the VMF1 2° × 2.5° (top) and VMF3 5° × 5° (middle)/1° × 1°

(bottom) grids. The blue triangles and black circles in the right panels denote the HCHMF-0 and HCHMF-2 models, respectively. The green pluses represent the height difference between station height and corresponding orography height

except for eight stations (denoted using red circles in Fig. 7). This will be further discussed in the next section.

4 Discussion

Compared with the Niell model, the accuracies of the hydrostatic delay mapping functions using the HCHMF-0 and HCHMF-2 models have been shown to be better. In this section, some factors that affect the performance are further discussed.

4.1 Benefits and importance of the HCHMF-2 model

As shown in Fig. 7, the performances of the HCHMF-0 and HCHMF-2 models are similar for most IGS stations. Is it

still necessary to generate the HCHMF-2 model? To answer this question, we conducted the following analysis as an example. We generated 5° × 5° gridded mapping functions from the monthly averaged ERA5 data in 2015 using the VMF3 5° × 5° orography file, named ‘orography_ell_5 × 5’. Meanwhile, the site-dependent mapping functions using the monthly averaged ERA5 data in 2015 were calculated directly at 258,121 simulated sites, located at 0.5° × 0.5° grids 1.5 km above MSL, that is, every 0.5° in the longitudinal and latitudinal directions. Then, we applied the HCHMF-0 and HCHMF-2 models to the gridded mapping functions and compared them with the site-dependent mapping functions.

Figure 8 shows the RMS of the monthly SPD errors at the 3° elevation angle in 2015 on a global 0.5° × 0.5° grid for the two improved models, and the distribution of the differences for HCHMF-2 minus HCHMF-0. Compared with

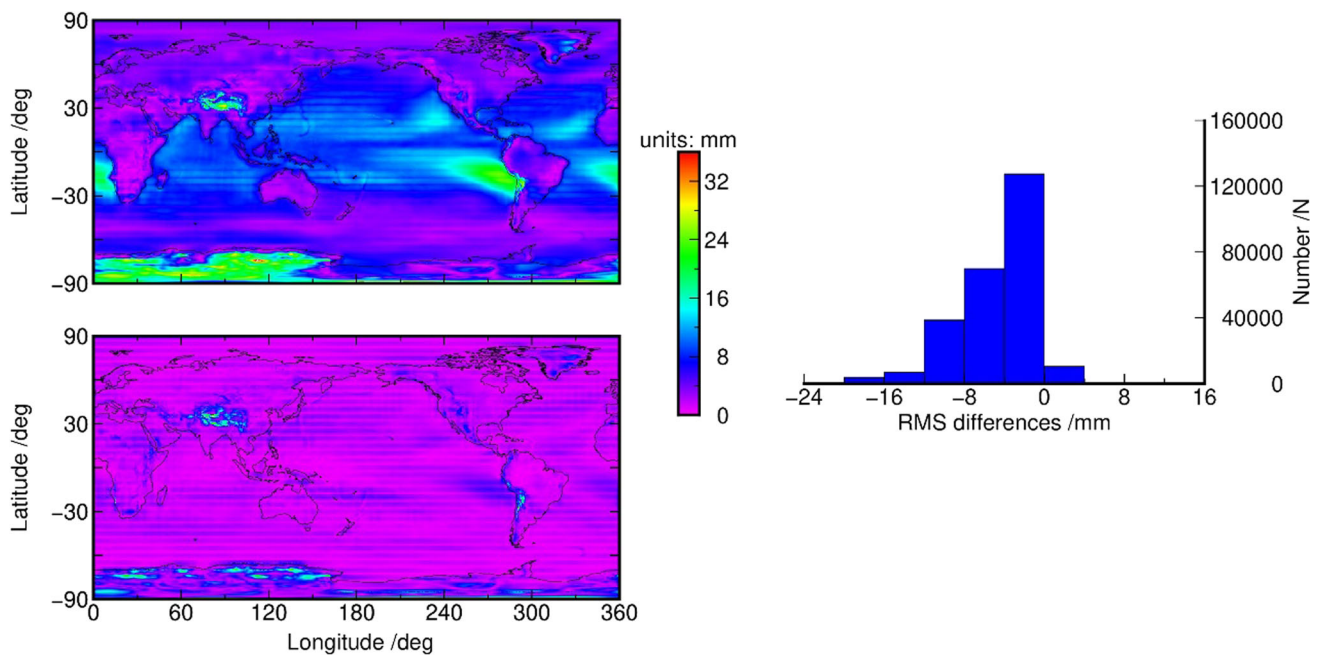


Fig. 8 RMS of the monthly SPD errors in 2015 at the 3° elevation angle for stations distributed in $0.5^\circ \times 0.5^\circ$ grids using the HCHMF-0 (top) and HCHMF-2 (bottom) models, together with the distribution of the

RMS differences between the two models (right). The colour bar in the left panels represents the RMS value. Right panel: X label represents the RMS differences, and Y label denotes the number of simulated sites

the HCHMF-2 model, the RMS of the HCHMF-0 model becomes larger for more than 95% of the grid points. Additionally, the RMS increases by more than 8 mm for 19% of the grid points, mainly located in the Tibetan Plateau, East Antarctica, Middle Andes and islands in the Atlantic Ocean and Pacific Ocean. This is consistent with the results shown in Fig. 7 that the accuracies of the HCHMF-0 model are worse than those of the HCHMF-2 model at several stations, with height differences of approximately 0.7–1.5 km. Considering the rule of thumb that GNSS station height error is one-fifth of the troposphere delay error at the lowest elevation angle (Boehm et al. 2006b; Zus et al. 2015), such improvement is important for precise GNSS applications, for example, the establishment of a terrestrial reference frame based on space techniques (Altamimi et al. 2016; Blewitt et al. 2010; Deng et al. 2016), which is particularly dependent on using mid-ocean geodetic stations to bridge vast ocean surfaces. These results validate the effectiveness of the HCHMF-2 model, and such effects will become even more important when more stations are installed in these areas.

4.2 Unified model coefficients for VMF1 and VMF3 grids

Due to the different strategies in calculating the mapping function coefficients b and c in VMF1/VMF3, we calculated different height correction coefficients of the HCHMF-2 model for the VMF1/VMF3 grids (hereafter called the VMF1

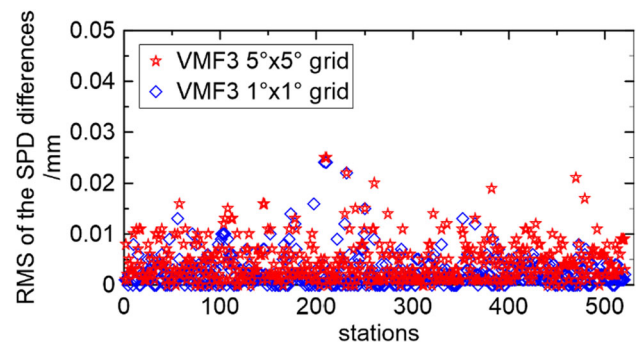


Fig. 9 RMS of the 6-hourly SPD differences in 2015 at the 3° elevation angle between the VMF1 and VMF3 HCHMF-2 models when applied to the VMF3 $5^\circ \times 5^\circ$ and $1^\circ \times 1^\circ$ grids. The red stars and blue squares represent the differences for VMF3 $5^\circ \times 5^\circ$ and $1^\circ \times 1^\circ$ grids, respectively

HCHMF-2 model and VMF3 HCHMF-2 model, respectively). Can we ignore the differences and provide one unified model for VMF1/VMF3 grids? To answer this question, we applied the VMF1 HCHMF-2 model to the VMF3 $1^\circ \times 1^\circ$ and $5^\circ \times 5^\circ$ grids in 2015 and compared them with the results using the VMF3 HCHMF-2 model. Figure 9 shows the RMS of the 6-hourly SPD differences at the 3° elevation angle for 521 stations between the VMF1 and VMF3 HCHMF-2 models. Clearly, all the differences are smaller than 0.03 mm. Thus, it is feasible to ignore the differences in calculating hydrostatic coefficients b and c in VMF1/VMF3 and generate one unified height correction model.

Table 2 Details of three experiments, differentiated in the spatial resolution of the height correction model and mapping function, undertaken in evaluating the impacts of the height correction model’s spatial resolution

Experiments	Spatial resolution of height correction model	Spatial resolution of mapping functions
HCM5_MF5	5° × 5°	5° × 5°
HCM5_MF1	5° × 5°	1° × 1°
HCM1_MF1	1° × 1°	1° × 1°

4.3 Resolution of height correction models

The spatial resolution of the height correction model calculated in Sect. 2 is 5° × 5°. Can we further improve the accuracies by enhancing the spatial resolution of the HCHMF-2 model? We designed three experiments (HCM5_MF5, HCM5_MF1 and HCM1_MF1), listed in Table 2, to analyse the impact of the height correction model resolution. To avoid the impact of the differences between the data and methods adopted in this analysis, as well as in calculating VMF1/VMF3, the monthly height correction models and mapping functions in 2015 are all calculated by our own ray-tracing techniques. In addition, the mapping functions calculated directly at 521 sites from the monthly averaged ERA5 data are taken as reference.

Figure 10 shows the RMS of the monthly SPD errors in three experiments at the 3° elevation angle and the average RMS within five height difference intervals. Compared with the results in Fig. 6, an additional improvement of approximately 5–10 mm is achieved for the HCM5_MF5 and HCM5_MF1 experiments after removing differences in the NWM data and data processing strategies adopted. By improving the height correction model’s spatial resolution to 1° × 1°, an additional decrease in the RMS can be achieved, especially for those stations with heights between 0.5 and 2 km above MSL. This suggests that if time permits, a 1° × 1° height correction model would be a better choice. Moreover, compared with the results in the first two experiments, the resolution of the tropospheric mapping function plays an important role when the height differences are smaller than 1.0 km, where most of the permanent stations are located. Thus, the contribution of the refined height correction model resolution is limited when applied to the VMF3 5° × 5° grid.

4.4 Impact of polynomial degrees for the coefficient *a*

In the previous analysis, we modelled the coefficient *a* with a quadratic polynomial. What about the performance

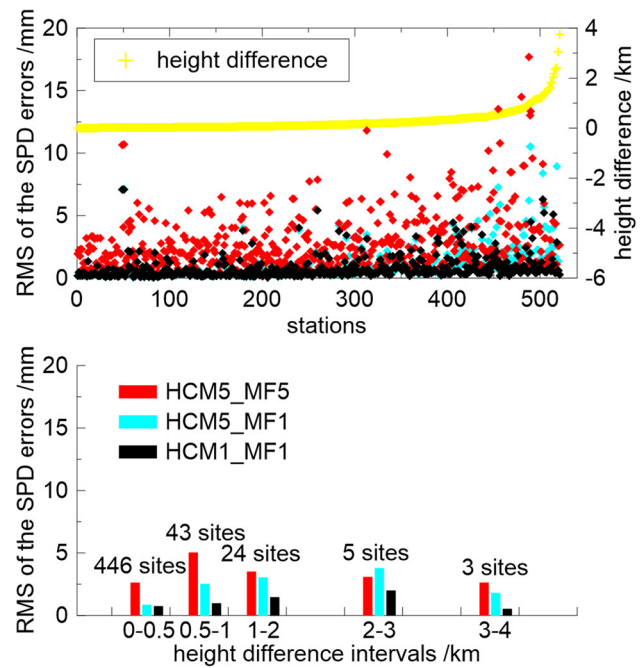


Fig. 10 RMS of the monthly SPD errors in 2015 (top) at the 3° elevation angle in three experiments, and the average RMS for stations within five height difference intervals (bottom). The yellow pluses denote the difference between station height and corresponding orography height

if adjusting the polynomial degree? To analyse this problem, we modelled the coefficient *a* with linear, quadratic and cubic polynomials, indicated as HCHMF-1, HCHMF-2 and HCHMF-3, respectively, and then recalculated the global gridded coefficients of 5° × 5° using ERA5 monthly data in 2015. The global average and maximum RMS of the monthly SPD residuals in 2015 at the 3° elevation angle for each height after fitting the coefficients are shown in Fig. 11. Clearly, the HCHMF-1 model, with a maximum RMS of 10.4 mm when the height difference reaches up to 1 km, has the worst performance. Compared with the results using HCHMF-2 however, the improvements using the HCHMF-3 model are not very significant. Detailed comparisons at all grid points (Table S1 in the supplementary material) show that the differences in the RMS of the monthly SPD residuals in 2015 between the HCHMF-2 and HCHMF-3 models are nearly all within 3 mm, and the maximum difference is 3.8 mm. Compared with the HCHMF-2 model, most grid points exhibit an increase in the RMS using the HCHMF-1 model, and the largest increase reaches up to approximately 8 mm. In contrast, only five grid points exhibit a reduction larger than 3 mm (Table S2 in the supplementary material). Hence, to balance both accuracy and complexity, we select the quadratic form as the suitable expression for the coefficient *a*.

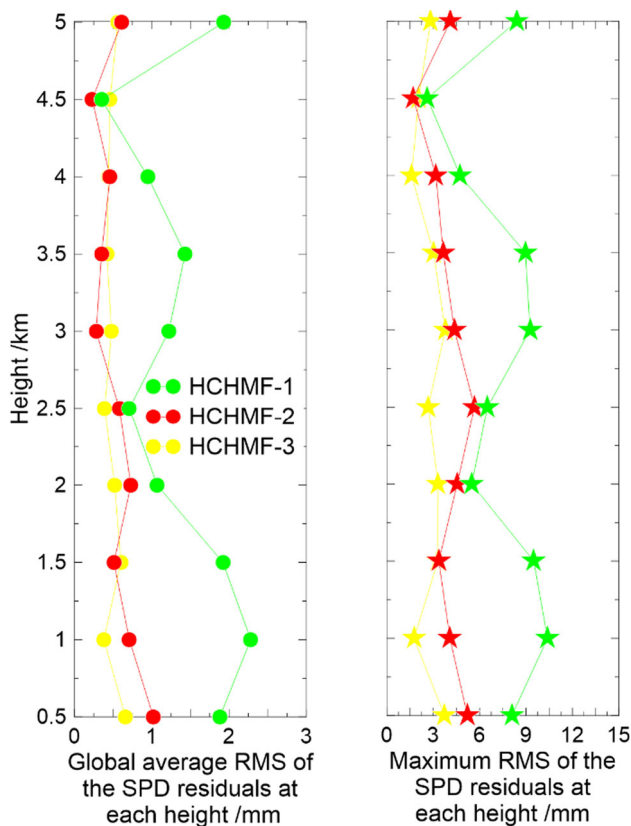


Fig. 11 Global average (left) and maximum (right) RMS of the monthly SPD residuals in 2015 at the 3° elevation angle at each height for HCHMF-1, HCHMF-2 and HCHMF-3. The different colours represent the different models (green: HCHMF-1, red: HCHMF-2, yellow: HCHMF-3)

5 Conclusions

In this analysis, an improved height correction model (HCHMF-2: Height Correction of Hydrostatic Mapping Function-2) for hydrostatic mapping functions is proposed and its accuracy analysed. Compared with the commonly used Niell model, the variation in coefficient a with respect to height is modelled quadratically in the improved model, while the spatial and temporal variations in coefficients are also considered. Our improved model shows good performance when applied to the VMF1/VMF3 grids. The accuracies are improved at most stations, especially at those stations with large height differences with respect to model orography. The improvements at the 3° elevation angle can reach up to 29.5 mm, 18.7 mm and 16.4 mm for the VMF1 $2^\circ \times 2.5^\circ$, VMF3 $5^\circ \times 5^\circ$ and $1^\circ \times 1^\circ$ grids, respectively. Due to a coarser resolution, improvements for the VMF1 $2^\circ \times 2.5^\circ$ and VMF3 $1^\circ \times 1^\circ$ grids are more evident than those for the VMF3 $5^\circ \times 5^\circ$ grid. In addition, one unified height correction model can be provided for the VMF1/VMF3 mapping functions, and the performances can be slightly improved by improving the resolution of height corrections

if time permits. Considering superior internal accuracies, such performance might also be improved by adopting the same NWM and data processing strategies in calculating the height correction model and mapping functions. Similar to the height correction model of the hydrostatic mapping function, the height correction model of the wet mapping function is also important for modelling wet tropospheric delays. In the future, the height correction model for the wet mapping function will be investigated and adopted, together with the height correction model for the hydrostatic mapping function in GNSS data processing when adopting gridded tropospheric mapping functions. Empirical models for the coefficients, with acceptable loss of accuracy, will also be investigated in the future for convenient use in GNSS data processing.

Supplementary Information The online version contains supplementary material available at <https://doi.org/10.1007/s00190-022-01677-y>.

Acknowledgements We thank the European Centre for Medium-Range Weather Forecasts (ECMWF) for providing numerical weather model (NWM) products and the Department of Geodesy and Geoinformation, TU Wien for providing the Vienna Mapping Function (VMF1/VMF3) data. This research is funded by the National Key Research Program of China ‘Collaborative Precision Positioning Project’ (No. 2016YFB0501900), the Key Research and Development Plan of Hubei Province (No. 2021EHB001), the National Natural Science Foundation of China (No. 42171141, No. 42104019) and the Key Laboratory of Geospace Environment and Geodesy, Ministry of Education, Wuhan University (20-01-10). The corresponding author is supported by the Youth Innovation Promotion Association CAS.

Author contributions WD proposed the idea, and wrote the manuscript; XQ developed the software, and designed the experiment; FT and YY contributed to discussion of the idea and helped with writing; TT, YZ and SL processed the data and analysed the results. All authors reviewed the manuscript.

Data availability The NWM products are available at <https://cds.climate.copernicus.eu/>. The VMF1/VMF3 data are available in the repository https://vmf.geo.tuwien.ac.at/trop_products/GNSS/.

Declarations

Conflict of interest The authors declare no conflicts of interest.

References

- Altamimi Z, Rebischung P, Métivier L, Collilieux X (2016) ITRF2014: a new release of the international terrestrial reference frame modeling nonlinear station motions. *J Geophys Res Solid Earth* 121(8):6109–6131. <https://doi.org/10.1002/2016JB013098>
- Blewitt G, Altamimi Z, Davis J, Gross R, Kuo CY, Lemoine FG, Moore AW, Neilan RE, Plag HP, Rothacher M, Shum CK, Sideris MG, Schöne T, Tregoning P, Zerbini S (2010) Geodetic observations and global reference frame contributions to understanding sea-level rise and variability. In: Church JA, Woodworth PL, Aarup P, Wilson WL (eds) *Understanding sea-level rise and variability*. Wiley-Blackwell, Oxford, pp 256–284

- Boehm J, Schuh H (2004) Vienna mapping functions in VLBI analyses. *Geophys Res Lett* 31:1603. <https://doi.org/10.1029/2003GL018984>
- Boehm J, Niell A, Tregoning P, Schuh H (2006a) Global mapping function (GMF): a new empirical mapping function based on numerical weather model data. *Geophys Res Lett.* <https://doi.org/10.1029/2005GL025546>
- Boehm J, Werl B, Schuh H (2006b) Troposphere mapping functions for GPS and very long baseline interferometry from European Centre for Medium-Range Weather Forecasts operational analysis data. *J Geophys Res.* <https://doi.org/10.1029/2005JB003629>
- Boehm J, Kouba J, Schuh H (2009) Forecast Vienna Mapping Functions 1 for real-time analysis of space geodetic observations. *J Geod* 83:397–401. <https://doi.org/10.1007/s00190-008-0216-y>
- Collins JP, Langley RB (1997) A tropospheric delay model for the user of the wide area augmentation system. University of New Brunswick, Fredericton, Department of Geodesy and Geomatics Engineering
- Davis J, Herring T, Shapiro I, Rogers A, Elgered G (1985) Geodesy by radio interferometry: effects of atmospheric modeling errors on estimates of baseline length. *Radio Sci* 20(6):1593–1607. <https://doi.org/10.1029/RS020i006p01593>
- Deng L, Jiang W, Li Z, Chen H, Wang K, Ma Y (2016) Assessment of second- and third-order ionospheric effects on regional networks: case study in China with longer CMONOC GPS coordinate time series. *J Geod* 91:207–227
- Dousa J, Elias M (2014) An improved model for calculating tropospheric wet delay. *Geophys Res Lett* 41:4389–4397. <https://doi.org/10.1002/2014GL060271>
- Hersbach, H, Bell B, Berrisford P, Biavati G, Horányi A, Muñoz Sabater J, Nicolas J, Peubey C, Radu R, Rozum I, Schepers D, Simmons A, Soci C, Dee D, Thépaut J-N (2019) ERA5 monthly averaged data on pressure levels from 1979 to present. Copernicus Climate Change Service (C3S) Climate Data Store (CDS). (Accessed on < 19-009-2019>). <https://doi.org/10.24381/cds.6860a573>
- Kouba J (2008) Implementation and testing of the gridded Vienna mapping function 1 (VMF1). *J Geod* 82(4–5):193–205. <https://doi.org/10.1007/s00190-007-0170-0>
- Lagler K, Schindelegger M, Boehm J, Krásná H, Nilsson T (2013) GPT2: empirical slant delay model for radio space geodetic techniques. *Geophys Res Lett* 40(6):1069–1073. <https://doi.org/10.1002/grl.50288>
- Landskron D, Boehm J (2018) VMF3/GPT3: refined discrete and empirical troposphere mapping functions. *J Geod* 92(4):349–360. <https://doi.org/10.1007/s00190-017-1066-2>
- Lou Y, Huang J, Zhang W, Liang H, Zheng F, Liu J (2018) A new zenith tropospheric delay grid product for real-time PPP applications over China. *Sensors* 18:65. <https://doi.org/10.3390/s18010065>
- Mahoney M (2005) A discussion of various measures of altitude. NASA Jet Propuls Lab. <http://mtp.mjhoneynet/www/notes/altitude/altitude.html>
- Niell A (1996) Global mapping functions for the atmosphere delay at radio wavelengths. *J Geophys Res* 101(B2):3227–3246
- Niell A (2000) Improved atmospheric mapping functions for VLBI and GPS. *Earth Planets Space* 52(10):699–702. <https://doi.org/10.1186/BF03352267>
- Ning T, Wang J, Elgered G, Dick G, Wickert J, Bradke M, Sommer M, Querel R, Smale D (2016) The uncertainty of the atmospheric integrated water vapour estimated from GNSS observations. *Atmos Meas Tech* 9:79–92. <https://doi.org/10.5194/amt-9-79-2016>
- Qu X, Li Z, An J, Ding W (2015) Characteristics of second-order residual ionospheric errors in GNSS radio occultation and its impact on inversion of neutral atmospheric parameters. *J Atmos Terr Phys* 130–131:159–171. <https://doi.org/10.1016/j.jastp.2015.05.016>
- Rüeger J M (2002) Refractive index formulae for radio waves. In: Proceedings of the FIG technical program; FIG XXII International Congress, Washington, DC
- Urquhart L, Nievinski FG, Santos MC (2014) Assessment of troposphere mapping functions using three-dimensional ray-tracing. *GPS Solut* 18:345–354
- World Meteorological Organization (2012) General Meteorological Standards and Recommended Practices. Basic Documents No. 2. WMO Technical Regulations, WMO-No. 49
- Zhang H, Yuan Y, Li W (2021) An analysis of multisource tropospheric hydrostatic delays and their implications for GPS/GLONASS PPP-based zenith tropospheric delay and height estimations. *J Geod* 95:83. <https://doi.org/10.1007/s00190-021-01535-3>
- Zus F, Dick G, Dousa J, Wickert J (2015) Systematic errors of mapping functions which are based on the VMF1 concept. *GPS Solut* 19(2):277–286. <https://doi.org/10.1007/s10291-014-0386-4>

Springer Nature or its licensor (e.g. a society or other partner) holds exclusive rights to this article under a publishing agreement with the author(s) or other rightsholder(s); author self-archiving of the accepted manuscript version of this article is solely governed by the terms of such publishing agreement and applicable law.